J. Fluid Mech. (1984), *vol.* 144, *pp.* 191–215
Printed in Great Britain

Flow past wing–body junctions

By F. T. SMITH
Mathematics Department, University College, Gower Street, London, WC1E 6BT

AND J. GAJJAR
N.M.I. Ltd, Teddington, Middx TW11 0JJ

(Received 29 June 1983 and in revised form 2 March 1984)

The three-dimensional laminar flow past a junction formed by a thin wing protruding normally from a locally flat body surface is considered for wings of finite span but short or long chord. The Reynolds number is taken to be large. The leading-edge interaction for a long wing has the triple-deck form, with the pressure due to the wing thickness forcing a three-dimensional flow response on the body surface alone. The same interaction describes the flow past an entire short wing. Linearized solutions are presented and discussed for long and short two-dimensional wings and for certain three-dimensional wings of interest. The trailing-edge interaction for a long wing is different, however, in that the three-dimensional motions on the wing and on the body are coupled together and in general the coupling is nonlinear. Linearized properties are retrieved only for reduced chord lengths. The overall flow structure for a long wing is also discussed, including the traditional three-dimensional corner layer, which is shown to have an unusual singular starting form near the leading edge. Qualitative comparisons with experiments are made.

1. Introduction

The three-dimensional motion of fluid past a wing–body junction is of much concern in aerodynamics, with regard to both the local and the global scale of the viscous effects produced and, in particular, to any pronounced secondary flows set up. As has proved to be the case in planar wing calculations, understanding of these effects and their scales may form a significant element in numerical schemes, addressing the Navier–Stokes equations or approximations for flow past an entire aircraft for instance, and the question arises of whether there can be an important influence on the aircraft performance overall or not. As well as the need to know the pressures and stresses exerted on a wing–body junction in flight, there is also the closely allied difficulty of determining the interference and interaction from the side wall when a planar wing model is placed in a wind tunnel. A number of interesting experimental studies of basically symmetric flow near wing–body-junction models have been made (Peake, Galway & Rainbird 1965; East & Hoxey 1968; Shabaka & Bradshaw 1981), usually for a very blunt, e.g. circular, wing protruding normally from a flat body surface. A common feature observed experimentally is the occurrence of three-dimensional separation upstream, with a curved separation line present on the body surface ahead of the wing.

Such truly nonlinear and complicated flowfields, involving three-dimensional boundary-layer collisions and often turbulence, for example, would seem of course to be well beyond the realms of much analysis. Indeed they appear rather remote

from the basic, perhaps most obvious, model we consider below, namely the junction formed by a flat body surface and a *thin* symmetric two- or three-dimensional wing of finite chord. Nevertheless it is found that certain of the theoretical properties that emerge are not far removed from the experimental observations for blunt wings, in qualitative terms at least, including the nature of the motion upstream and the suggested separation line there. Furthermore the model geometry discussed would seem to be more closely linked with the junctions of real life than is that associated with the similarity solution for flow along a streamwise corner, which has received much attention (e.g. Zamir 1968; Rubin & Grossman 1971; Desai & Mangler 1974). Lastly, we believe that an understanding of the flow past the model geometry here may be of benefit to the understanding and control of the complex flows that occur in practice. The theory below is concerned initially with the flow features arising near the start of the junction, that is, near the *leading edge* of a long wing or for an *entire* short wing. The incident boundary layer on the body surface is driven by the locally uniform external stream, is well-formed, attached and planar, and so in a sense its influence dominates the inviscid–viscous interaction between the flow on the wing and the flow on the body surface. For the attached Blasius boundary layer just forming on the wing is much thinner. The interaction provoked then has the triple-deck form, with the motion past the thin wing provoking, on the body surface, an unknown pressure force which interacts with the unknown displacement there. This causes the boundary layer on the body surface to become three-dimensional and to exhibit upstream influence. Nonlinearity results if the typical slope of the wing in the interaction stage is of order $Re^{-\frac{1}{4}}$, where Re is the large Reynolds number: see §2. For thinner wings, including the fundamental case of the flat plate where the Blasius displacement on the wing is responsible for the interaction, linearized analysis is possible and is described in §3. Linearized results are given in §§3 and 4 for two- and three-dimensional wings respectively, examples of the latter being swept wings and tapered wings.

Further comments are presented in §5, along with a study of the trailing edge of the junction. The model problems studied here have possible relevance also to certain other strongly three-dimensional motions, including the flow past fins, tail–body junctions, missiles, fishes, bridges, past high-rise buildings and in branching flow in pipes. An interesting feature is that even the thin wing can provoke a secondary-flow component of velocity which is comparable to the streamwise component near the body surface. Although for a very thin wing this nonlinear feature can be suppressed somewhat in the initial leading-edge interaction, it persists in the subsequent trailing-edge interaction for any long wing. The trailing-edge adjustment is therefore always nonlinear, unless the wing is relatively short, as noted in §5. We believe that experimental and/or computational studies of (e.g.) the fundamental, flat-plate, wing–body-junction model here could be most illuminating. This is especially so in view of the inference, to be drawn from the investigation below, that the complicated effects observed in practice (see references above, also McDonald & Briley 1982; Kitchens *et al.* 1983; Mehta, Shabaka & Bradshaw 1982; Mehta *et al.* 1983) near wing–body junctions *may* well be caused to a large extent by the presence of three-dimensional inviscid–viscous interaction, even for turbulent flows.

In what follows the motion is taken to be laminar and steady and the fluid is assumed to be incompressible.

2. A thin planar wing

We start by discussing the fluid motion past a wing–body junction formed by a thin planar symmetric wing projecting normally from the aircraft body. The latter is taken to have a flat surface, since our initial concern is with the localized flow features; more-global features are considered later in §5. Moreover, the wing is placed at zero incidence to the oncoming mainstream, while the resultant motion is assumed to be symmetric about the wing's centreplane $y = 0$, for convenience, and so we need study only the upper half of the motion, $y \geqslant 0$. Here, in Cartesian coordinates x, y, z, the wing starts at $x = 0$ and is given (for all $z > 0$) by $y = \tilde{f}(x)$ for $x > 0$, $y = 0$ for $x < 0$, where the typical wing thickness $|\tilde{f}|$ is small in some sense, whereas the body occupies the flat surface $z = 0$ for all x, y. See the sketch in figure 1. The lengths (x, y, z) above and the corresponding velocity cmponents (u, v, w) are non-dimensionalized with respect to l_∞ and u_∞ respectively, where l_∞ is the characteristic lengthscale of the body, e.g. the streamwise distance from the aircraft nose to the leading edge of the wing, and u_∞ is the speed of the mainstream, which flows in the positive x-direction. The pressure is written $p_\infty + \rho u_\infty^2 p$, with p_∞ and ρ denoting the mainstream pressure and the fluid density respectively. The typical global Reynolds number is then $Re = u_\infty l_\infty \nu^{-1}$, where ν is the kinematic viscosity of the fluid, and Re is supposed to be large.

On an inviscid basis, with the above wing–body geometry, the uniform stream given by $u = 1$, $v = w = 0$ continues broadly undisturbed apart from a small $O(|\tilde{f}|)$ perturbation. Viscous effects alter the flow substantially, however, near the wing and body surfaces at least, where viscous–inviscid interaction must occur. There then appear to be two aspects to consider. First, sufficiently near the start of the junction, for small x, and for a sufficiently thin wing, the predominant interaction involves just the effect, on the flow close to the body surface, of the motion past the wing. The 'opposite' effect, that of the flow near the body surface on the flow near the wing, is much less. The reason for this is that for small x the boundary layer on the wing is only just formed and so is thin compared with the more developed $O(Re^{-\frac{1}{2}})$ thick oncoming boundary layer, on the body, which by contrast has its origins at an $O(1)$ distance ahead of the wing–body junction. Hence the wing's boundary layer is much the more attached one then and is less affected by a given size of induced pressure field than is the thicker boundary layer on the body. The latter layer must be the first to feel the effects of any interaction, and is the one where three-dimensional separation, for instance, is to be expected at first.

That brings us to the second main aspect, which concerns the type and scale of interaction. Nonlinear responses such as separation in an external developed boundary layer, whether three-dimensional (Smith, Sykes & Brighton 1977) or not, are controlled largely by the triple-deck interaction, as is well known. Formally, therefore, the critical size of induced pressure p, i.e. the smallest size that provokes a nonlinear interactive response in the body's boundary layer, is of order $Re^{-\frac{1}{4}}$, and the streamwise lengthscale invoked is $O(Re^{-\frac{3}{8}})$. This emphasizes initially the role played by a wing that produces an $O(Re^{-\frac{1}{4}})$ typical pressure field within a distance $O(Re^{-\frac{3}{8}})$ of its leading edge, since these are the triple-deck scales. There are perhaps two main categories of such wings to consider. One comprises wings of $O(1)$ chord length in x ('long wings'); the other comprises wings of chord length $O(Re^{-\frac{3}{8}})$ ('short wings'). The flow properties for other chord lengths tend to be covered by limiting cases of the above two. Now the pressure p induced near the leading edge or nose of a *long* thin wing depends mostly on the local wing shape there. For p is given by

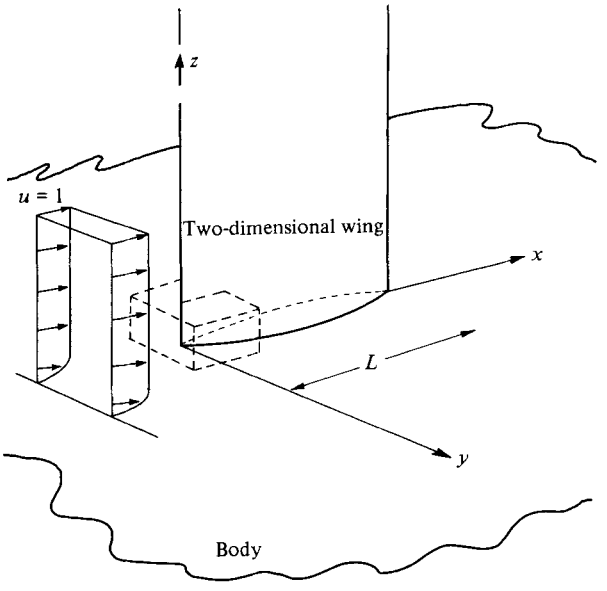

FIGURE 1. The junction formed by a thin symmetric two-dimensional wing of length L normal to the body surface ($z = 0$) and aligned with the oncoming two-dimensional uniform stream and body-surface boundary layer ($O(Re^{-\frac{1}{2}})$). The triple-deck 'box', describing the three-dimensional flow around the junction's leading edge for a long wing ($L = O(1)$), or about the entire junction for a short wing ($L = O(Re^{-\frac{3}{8}})$), is shown by dashed lines. See also figure 8.

the Cauchy–Hilbert integral of the wing's slope (see below) on an inviscid basis, and so near a leading edge p is predominantly proportional to the local wing slope, in addition to regular global contributions of order H, where H is the small maximum-thickness-to-chord ratio. Thus with a typical blunt nose of the parabolic form $y = \tilde{f}(x) \sim Hx^{\frac{1}{2}}(x \to 0+)$, for example, the induced pressure $p \propto Hx^{-\frac{1}{2}}$ predominantly as $x \to 0+$. So when x falls to $O(Re^{-\frac{3}{8}})$ the critical interactive pressure $O(Re^{-\frac{1}{4}})$ is reached if the maximum wing thickness H is $O(Re^{-\frac{7}{16}})$. In addition, the viscous boundary layer on such a wing has the Blasius form of thickness $O(Re^{-\frac{1}{2}}x^{\frac{1}{2}})$ $(x > 0)$ and so is always thinner than the wing thickness H in that case (see also §3) and has negligible effect to leading order. Another point of concern is the traditional nonlinear inviscid zone of non-uniformity near the leading edge (see e.g. Van Dyke 1964), but this is of extent $O(H^2) = O(Re^{-\frac{7}{8}})$, small compared with the $x \sim Re^{-\frac{3}{8}}$ interaction scale, and can be reasonably presumed to have negligible influence also. Local shapes other than the parabola can be regarded similarly. Thus if the shape $\tilde{f}(x) \sim Hx^n$ as $x \to 0+$ with $0 < n < 1$ for a blunt nose, then locally the pressure $p \propto Hx^{n-1}$, which tends to $O(HRe^{\frac{3}{8}(1-n)})$ in the triple-deck interaction scale, pointing to the critical thickness $H = O(Re^{-\frac{1}{8}(5-3n)})$ for nonlinear viscous–inviscid interaction. This is self-consistent provided that the $O(Re^{-\frac{1}{2}})$ displacement thickness of the wing's boundary layer remains negligible for all x of current interest, implying the restriction that $n > \frac{1}{3}$. Conversely, therefore, if $n \leqslant \frac{1}{3}$ the displacement thickness then has a leading-order or even dominant influence downstream on the induced pressure, although not necessarily within the interaction length (depending again on the local wing shape there). The same crossover between the influence of the wing thickness and that of its viscous boundary layer can occur if, for a given value of the shape index n, the wing thickness H is below the critical thickness determined previously; in that case only a linearized wing–body interaction is induced, since the pressure forcing due to

the flow past the wing is less than the critical triple-deck value needed for nonlinear interaction on the body surface. Examples are given in §3.

The central point overall is that the induced pressure from any planar blunt long wing is dominated by the local wing shape, and unaffected by the shape further downstream, as regards the wing–body interaction properties near the leading edge. On the other hand, the critical thickness for a *short* thin wing as defined at the start of this paragraph is always $O(Re^{-\frac{5}{8}})$, since then its typical slope, and hence its pressure effect from the Cauchy–Hilbert integral, is $O(Re^{-\frac{1}{4}})$, as required for significant interaction with the body's boundary layer. The above arguments have to assume suitable smoothness of the thin wing surface of course and essentially attached flow thereon. Attached flow, with a thin boundary layer, is achieved if the trailing edge is cusped, for instance, but it becomes open to question for less sharp trailing edges, especially blunt ones, where local small separations, if not worse, can occur. Nevertheless, for the long thin wing the leading-edge flow properties are dominated so much by the nose shape that they are still unaltered to leading order by any breakaway separation from the wing downstream, while for the short wing, trailing-edge separation can remain a relatively confined phenomenon. So the attached flow restriction, applied for convenience to the flow around the wing, can be relaxed if necessary.

Two-dimensional flow alone past the thin short or long wing above produces in consequence an $O(Re^{-\frac{1}{4}})$ pressure field dependent only on x and y. This holds good for distances z greater than $O(Re^{-\frac{3}{8}})$ from the body surface $z = 0$, but not when z is $O(Re^{-\frac{3}{8}})$, since at such distances the three-dimensional triple-deck interaction takes place, with the $O(Re^{-\frac{1}{4}})$ pressure provoking within the body boundary layer an $O(Re^{-\frac{5}{8}})$ displacement comparable to the local wing thickness. The three-dimensional linearized potential flow in the upper deck just outside the boundary layer then, for distances z of order $Re^{-\frac{3}{8}}$, is governed by Laplace's equation $(\partial^2/\partial X^2 + \partial^2/\partial Y^2 + \partial^2/\partial \bar{z}^2)\,\bar{p} = 0$ for the unknown reduced pressure $\bar{p}$ with the boundary conditions $\partial\bar{p}/\partial Y(X, 0+, \bar{z}) = -h\,\mathrm{d}^2 f/\mathrm{d}X^2$, $\partial\bar{p}/\partial\bar{z}(X, Y, 0+) = -\partial^2\delta(X, Y)/\partial X^2$ and $\bar{p}(X, Y, 0+) = P(X, Y)$, for (respectively) tangential flow on the scaled local wing surface $Y = h\,Re^{-\frac{1}{4}} f(X)$ and to match the body's unknown scaled displacement thickness $\delta(X, Y)$ and unknown scaled pressure $P(X, Y)$. Here $(x, y, z) = Re^{-\frac{3}{8}}(X, Y, \bar{z})$, $p = Re^{-\frac{1}{4}}\bar{p}$ give the upper-deck scalings and $\bar{p}$, f, δ, P and the reduced wing thickness parameter h are generally of order unity, while the domain of interest is $-\infty < X < \infty$, $0 < Y < \infty$, $0 < \bar{z} < \infty$ by symmetry. The solution for the pressure $\bar{p}$ here can be viewed as consisting of two parts: (*a*) the two-dimensional wing solution given by the single Cauchy–Hilbert integral

$$\bar{p}(X, Y, \bar{z}) = -\frac{h}{\pi}\int_{-\infty}^{\infty} \frac{\mathrm{d}f(\xi)}{\mathrm{d}\xi}\frac{(X-\xi)\,\mathrm{d}\xi}{(X-\xi)^2 + Y^2}, \tag{2.1}$$

which has the advantage of producing no displacement on the body surface $\bar{z} = 0+$; and (*b*) the three-dimensional solution corresponding to the unknown displacement $\delta(X, Y)$ on the body alone, with the symmetry of δ with respect to Y adding no extra displacement on the wing $Y \to 0+$. The combination of (*a*) and (*b*) achieves the desired wing and body inviscid conditions, and hence we have the forced pressure–displacement relation

$$P(X, Y) = -\frac{h}{\pi}\int_{-\infty}^{\infty} \frac{\mathrm{d}f(\xi)}{\mathrm{d}\xi}\frac{(X-\xi)\,\mathrm{d}\xi}{(X-\xi)^2 + Y^2} + \frac{1}{2\pi}\int_{-\infty}^{\infty}\int_{-\infty}^{\infty} \frac{(\partial^2\delta/\partial\xi^2)\,\mathrm{d}\xi\,\mathrm{d}\eta}{[(X-\xi)^2 + (Y-\eta)^2]^{\frac{1}{2}}}. \tag{2.2a}$$

This relation then controls the flow induced on the body surface, and the unknowns P and δ. That flow involves the main and lower decks, being governed primarily by

the lower-deck properties where $z = \mathrm{Re}^{-\frac{5}{8}}Z$ and the three-dimensional boundary-layer equations

$$\frac{\partial U}{\partial X}+\frac{\partial V}{\partial Y}+\frac{\partial W}{\partial Z}=0, \tag{2.2b}$$

$$U\frac{\partial U}{\partial X}+V\frac{\partial U}{\partial Y}+W\frac{\partial U}{\partial Z}=-\frac{\partial P}{\partial X}(X,\,Y)+\frac{\partial^2 U}{\partial Z^2}, \tag{2.2c}$$

$$U\frac{\partial V}{\partial X}+V\frac{\partial V}{\partial Y}+W\frac{\partial V}{\partial Z}=-\frac{\partial P}{\partial Y}(X,\,Y)+\frac{\partial^2 V}{\partial Z^2} \tag{2.2d}$$

apply, with the usual triple-deck scalings (Smith *et al.* 1977). The boundary conditions here are

$$U=V=W=0 \quad \text{at} \quad Z=0, \tag{2.2e}$$

$$U\sim\lambda(Z-\delta(X,\,Y)), \quad V\to 0 \quad \text{as} \quad Z\to\infty, \tag{2.2f}$$

$$(U,\,V,\,W,\,P)\to(\lambda Z,0,0,0) \quad \text{as} \quad X\to-\infty, \tag{2.2g}$$

respectively for no slip on the flat body surface, for matching with the displaced main part of the $O(Re^{-\frac{1}{2}})$ boundary layer, and for joining with the planar boundary layer upstream. The constant λ is the incident $O(1)$ skin friction, taken to be unity henceforth for convenience. Also, by symmetry, $V=0$ at $Y=0$.

The viscous–inviscid three-dimensional flow interaction for the wing–body junction is given by the solution of (2.2*a–g*) for a prescribed wing shape $hf(X)$. It is noteworthy that the forcing ($\propto hf(X)$) which produces the interaction and three-dimensionality in the body's boundary layer comes from outside the boundary layer itself, which is a mechanism quite different from those in three-dimensional interactive flows (e.g. past humps) considered previously. The presence of the thin wing shape in the upper deck outside the boundary layer forces only a small pressure perturbation there, but this pressure when fed down through the body's boundary layer is enough to provoke the nonlinear response in the slower, lower-deck, flow close to the body surface. In that slower flow the wing shape plays hardly any further part, as it is relatively thin, except for the necessity of tangential flow at the wing surface, or in the present case the symmetry requirement $V=0$ at $Y=0$. The resultant problem is nonlinear in general and so requires a numerical treatment. Subsequently we consider the linearized versions, valid strictly if the wing-thickness parameter h is small, or for the basic problem of a wing which is a finite flat plate: see §3. Meanwhile it is worth remarking that the three-dimensional triple-deck interaction emphasized above does not cover all the features of the three-dimensional flow. Other small subregions of interest are present, including the thin $O(Re^{-\frac{11}{16}})$ (in y) boundary layer developing on the locally $O(Re^{-\frac{5}{8}})$ thick wing, and a small corner zone $O(Re^{-\frac{5}{8}})$ by $O(Re^{-\frac{5}{8}})$ (in y, z) where y- and z-diffusion are equally significant. All of these subregions are believed to be passive relative to the triple-deck interaction, however, which seems a bold assumption, perhaps, but which can be backed up physically. In particular, the wing's boundary layer is driven forward in a quasi-Blasius fashion, apart from in the corner zone and in the traditional leading-edge nonlinear inviscid zone for smaller x, and so does not affect (2.2*a–g*). Larger-scale regions of interest also arise, but only further downstream as discussed in §5, and these likewise have negligible effect on the fundamental problem (2.2*a–g*). Other more general sizes for the wing dimensions or for the incident planar boundary-layer thickness can also be accommodated, but these are merely limiting cases of the fundamental triple-deck problem, unless large-scale separation occurs, which is a case beyond our current scope. Accordingly we focus

attention on (2.2*a–g*) for a number of wing shapes $f(X)$, both short and long, in §§3 and 4, before considering larger-scale properties and trailing-edge effects in §5.

3. Linearized solutions for thin or flat planar wings

When the wing-thickness parameter h in (2.2*a*) is small, a linearized version of (2.2*a–g*) applies, and much of the analysis in Smith *et al.* (1977) on flow past humps can be taken over. To shorten matters we may work conveniently in terms of an 'effective hump shape' then, since the double Fourier transform in X and Y (for notation see Smith *et al.*) of (2.2*a*) gives

$$\frac{P^{**}(k,l)}{h} = -\frac{2k^2 f^*(k)}{k^2+l^2} - \frac{k^2 \delta^{**}(k,l)}{h(k^2+l^2)^{\frac{1}{2}}}. \tag{3.1}$$

Here $f^*(k)$ is the transform of $f(X)$ with respect to X, and δ stands for $-A$ in Smith *et al.* So a comparison with §3 of that paper shows that our linearized problem for a wing shape $hf(X)$ and flat surface $Z = 0$ corresponds to the linearized problem of flow over a hump given by $Z = hF(X, Y)$, where the effective hump shape F satisfies

$$F^{**}(k,l) = 2(k^2+l^2)^{-\frac{1}{2}} f^*(k). \tag{3.2}$$

The same analogue holds in the nonlinear regime, incidentally. The linearized solutions for the transforms we require then follow from Smith *et al.* In particular,

$$\frac{P^{**}(k,l)}{h} = \frac{2(\mathrm{i}k)^2 f^*(k)\,(k^2+l^2)^{-1}}{\Delta}, \tag{3.3a}$$

$$\frac{\delta^{**}(k,l)}{h} = \frac{2\gamma^{-\frac{4}{3}}(\mathrm{i}k)^{\frac{1}{3}} f^*(k)}{\Delta}, \tag{3.3b}$$

$$\left(\frac{\tau_X - 1}{h}\right)^{**}(k,l) = \frac{6\mathrm{Ai}(0)\,(\mathrm{i}k)^{\frac{2}{3}} f^*(k)}{(k^2+l^2)\,\Delta}\left[\frac{k^2+l^2}{\gamma^{\frac{4}{3}}} - \frac{l^2}{9\mathrm{Ai}^2(0)}\right], \tag{3.3c}$$

$$\frac{\tau_Y^{**}(k,l)}{h} = -\frac{2(\mathrm{i}l)\,(\mathrm{i}k)^{\frac{5}{3}} f^*(k)}{3\mathrm{Ai}(0)\,(k^2+l^2)\,\Delta}, \tag{3.3d}$$

$$\frac{D^{**}(k,l)}{h} = -\frac{2(\mathrm{i}l)\,(\mathrm{i}k) f^*(k)}{(k^2+l^2)\,\Delta}, \tag{3.3e}$$

where

$$\Delta = 1 + \gamma^{-\frac{4}{3}}(\mathrm{i}k)^{\frac{1}{3}}(k^2+l^2)^{\frac{1}{2}}$$

In (3.3) the functions $\tau_X \equiv \partial U/\partial Z(X, Y, 0)$ and $\tau_Y \equiv \partial V/\partial Z(X, Y, 0)$ denote the surface shear stresses in the X- and Y-directions, and $D(X, Y)$ satisfies $\partial D/\partial X = -\partial P/\partial Y$ and helps to describe the motion more removed from the body surface, since $V \sim D(X, Y)\,Z^{-1}$ for large Z.

Fast-Fourier-transform (FFT) calculations were used to determine the corresponding real quantities, and the results were checked on different grid sizes and integration ranges. The following short and long wing shapes were considered:

$$f(X) = X^{\frac{1}{2}} \exp(-X^2) \quad (X > 0) \quad \text{(long)}, \tag{3.4a}$$

$$f(X) = X^{\frac{1}{2}} (X > 0) \quad \text{(long)}, \tag{3.4b}$$

$$f(X) = X(1-X) \quad (0 < X < 1) \quad \text{(short)}, \tag{3.4c}$$

$$f(X) = X^{\frac{1}{2}}(1-X)^{\frac{1}{2}} \quad (0 < X < 1) \quad \text{(short)}, \tag{3.4d}$$

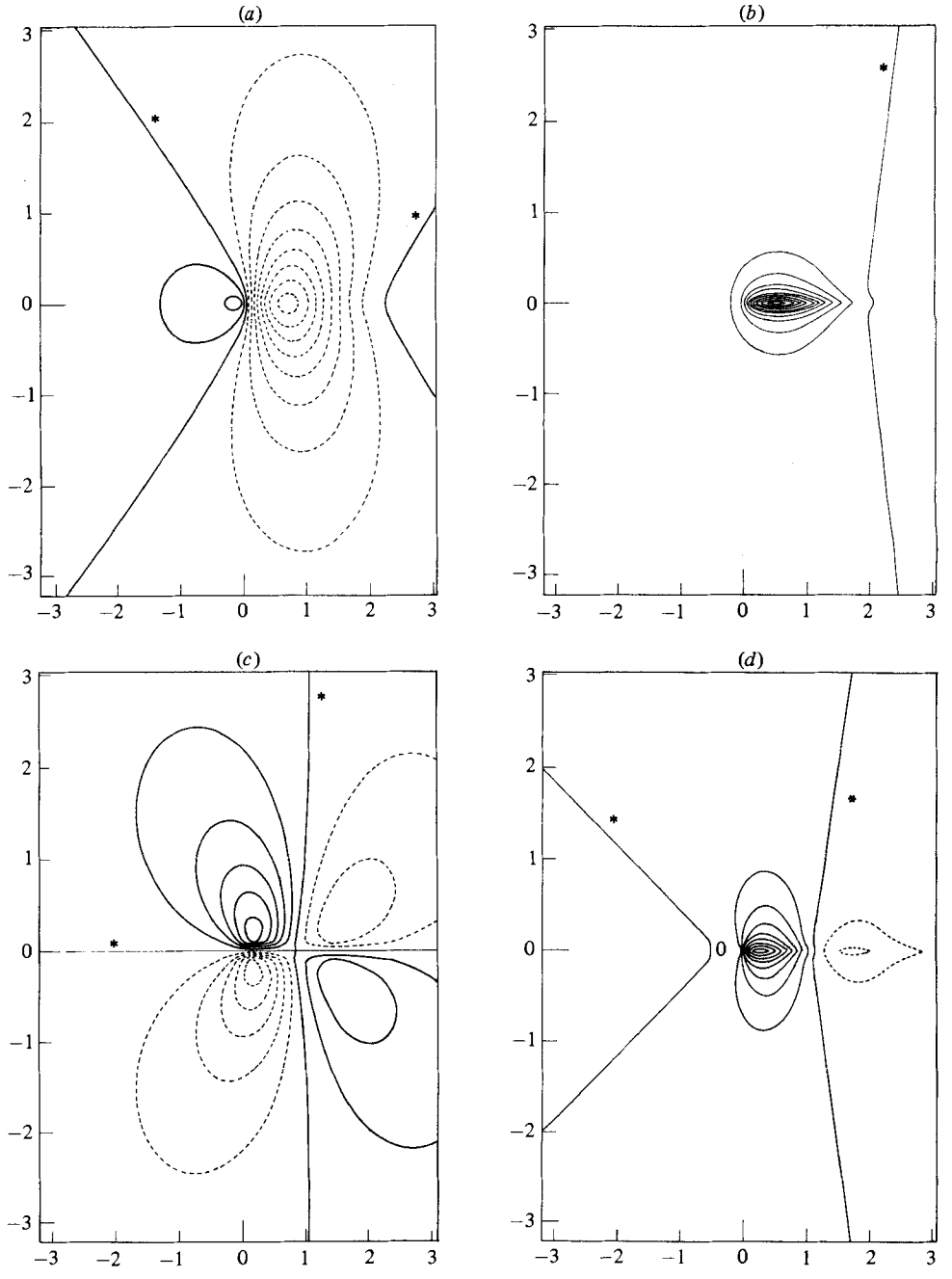

FIGURE 2. For caption see facing page.

with $f(X) \equiv 0$ otherwise. Their solution properties are presented in figures 2–5. It should be noted that rather extensive grids were needed to accommodate the far-field behaviour of (3.3*a–e*), especially for the long wing shapes. Results from different grids indicate that graphical accuracy is usually achieved, and our figures present the most accurate results obtained in each case, although some distortion persists in the farfields (see also (3.5) ff. below) and in the symmetry or antisymmetry of the

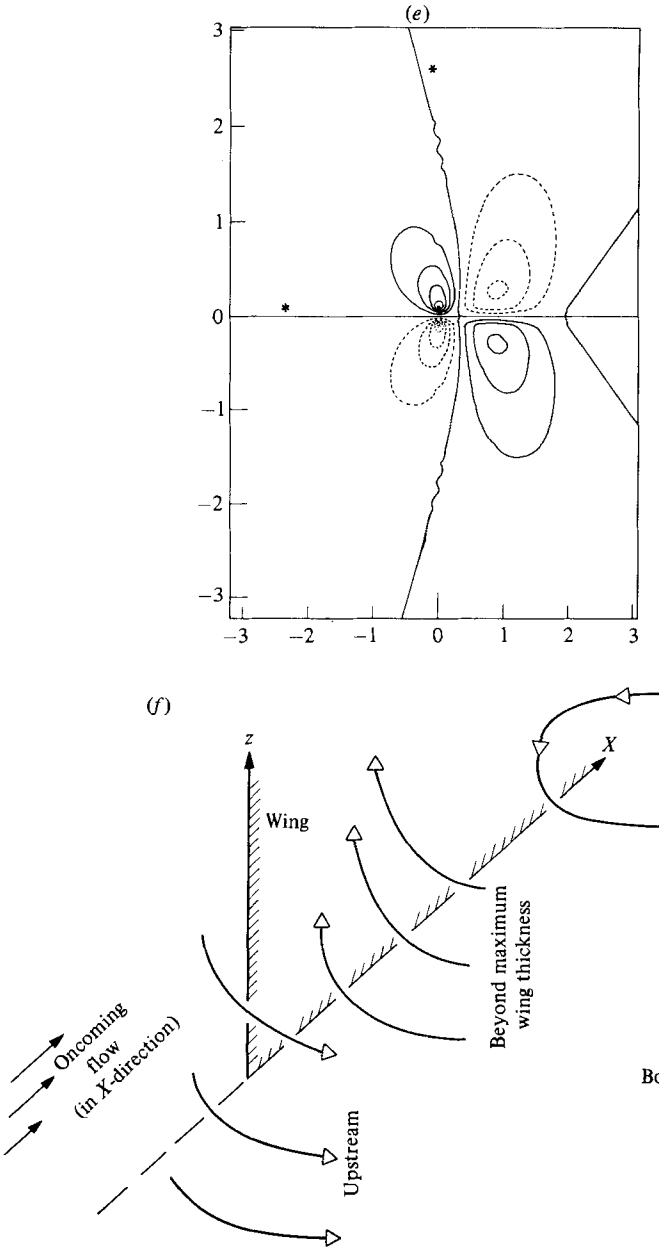

FIGURE 2. Linearized three-dimensional flow solutions, for the two-dimensional long wing–body junction of (3.4*a*), showing in (*a*)–(*e*) curves of constant P, $-\delta$, D, τ_X, τ_Y and in (*f*) the typical secondary flows and vortices produced by the two-dimensional wings. The axes in (*a*)–(*e*) are X, Y. The contour values for P are -0.14, -0.12, -0.10, -0.087, -0.070, -0.052, ± 0.035, ± 0.017, zero (marked *); for $-\delta$ they are zero (*), 0.10, 0.21, 0.31, 0.42, 0.52, 0.63, 0.73, 0.83, 0.94, 1.00; for D they are ± 0.064, ± 0.051, ± 0.038, ± 0.025, ± 0.013, zero (*); for τ_X they are ± 0.16, ± 0.078, zero (*), 0.23, 0.31, 0.39, 0.47, 0.55, 0.62; and those for τ_Y are ± 0.12, ± 0.099, ± 0.075, ± 0.50, ± 0.025, zero (marked *). – – –, negative values; ——, positive values. For the purposes of comparison and analytical checks, the far-field asymptotes for the contours of level zero are at slopes Y/X of ± 1 for P; ∞ for δ; 0 and ∞ for D, approximately 4.8 and -0.67 for τ_X; and approximately -2.4 and 1 for τ_Y. Here the asymptotic slopes for zero P, D, δ stem directly from (3.3*b*), (3.5*a*, *b*), while those for τ_X, τ_Y come from numerical evaluation of the real convolution integrals implied by (3.3*c*, *d*) when $k, l \to 0$.

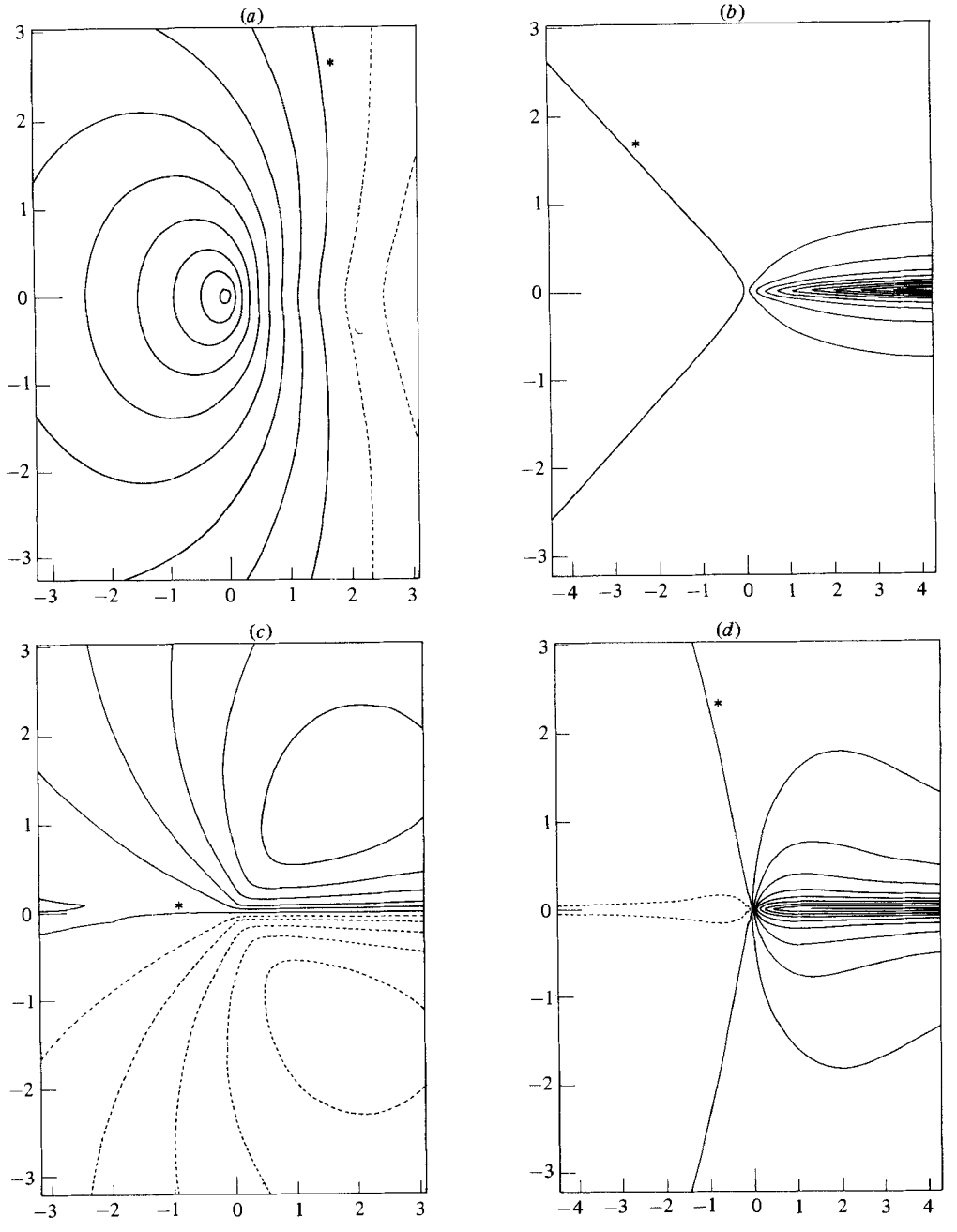

FIGURE 3. For caption see facing page.

solutions, as well as in a few local features, e.g. wiggles. Such distortions all shrink under grid refinement, but computer storage limitations have prevented us from removing them totally from the results. The grid sizes used for most of the figures in this paper had approximately 768 points in k with $-30 \leqslant k \leqslant 30$ and 512 points in l with $-25 \leqslant l \leqslant 25$.

The main features apparent in the flow solutions seem sensible physically and are broadly as follows. Upstream of the wing, along the symmetry line $Y = 0$, a common

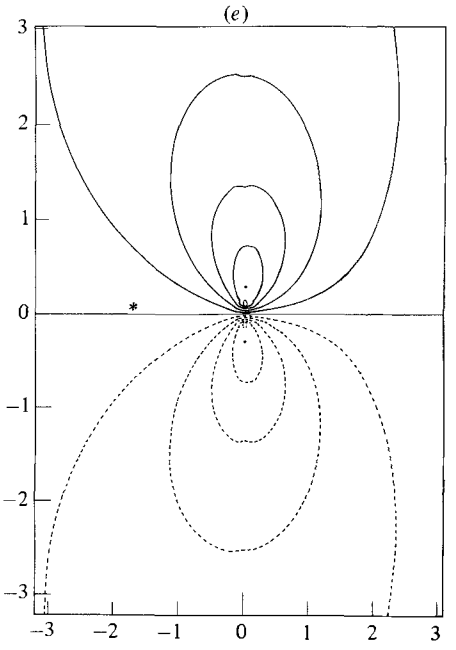

FIGURE 3. Linearized three-dimensional flow solutions for the long wing (3.4*b*), or for a flat-plate wing (see final paragraph of §3). Notation and general secondary flow are as in figure 2. The contour values for P, $-\delta$, D, τ_X, τ_Y are: (*a*) ± 0.068, ± 0.034, zero (*), 0.10, 0.14, 0.17, 0.20, 0.24, 0.27; (*b*) zero (*), 0.40, 0.80, 1.2, 1.6, 2.0, 2.4, 2.8, 3.2, 3.6, 4.0; (*c*) ± 0.19, ± 0.15, ± 0.12, ± 0.077, ± 0.039, zero (*); (*d*) ± 0.087, zero (*), 0.17, 0.26, 0.35, 0.44, 0.52, 0.61, 0.70, 0.79; (*e*) ± 0.15, ± 0.12, ± 0.09, ± 0.06, ± 0.03, zero (*).

occurrence is the rise in pressure and the associated drop in the X-shear stress τ_X. This is much like a two-dimensional flow response ahead of the effective hump shape. Associated with it there is a generally positive Y-shear stress τ_Y and Y 'edge velocity' D, as might be expected, but the displacement δ falls, which is a surprising feature at first sight. Thus fluid is forced away (in the Y-direction) from the symmetry line, but tends to be drawn (in the negative Z-direction) *towards* the body surface there, ready to negotiate the wing beyond. This and other initially unexpected properties of the displacement are caused by the pressure from the wing, contributing the f^* term in (3.1). The fluid can only go around the wing, not over it, in broad terms, and so there is here a significant difference from the flow past (and over) humps studied by Smith *et al.* (1977). Near the front of the wing there is a particularly marked fall in the displacement, in fact. As soon as the wing position is encountered, however, the displacement adjusts rather fast, rising to become positive eventually downstream; the pressure rises more rapidly, then falls rapidly to a minimum before slowly recovering; and the shear stress τ_X increases fairly abruptly to a maximum, followed also by a slower recovery downstream. So there the flow is accelerated, whilst the fluid ultimately is drawn back towards the symmetry line (τ_Y, $D > 0$) in the positive Z-direction. Trends roughly opposite to those near the wing's leading edge occur in the neighbourhood of the trailing edge for a short wing. The trailing edge acts like a sink for the three-dimensional flow, compared with the source-like role of the leading edge. See also §5 on trailing-edge effects. Finally, sufficiently far downstream the pressure overshoots to become positive again before decreasing back to zero, while the shear stress τ_X undershoots to a minimum, then increases to unity, and the

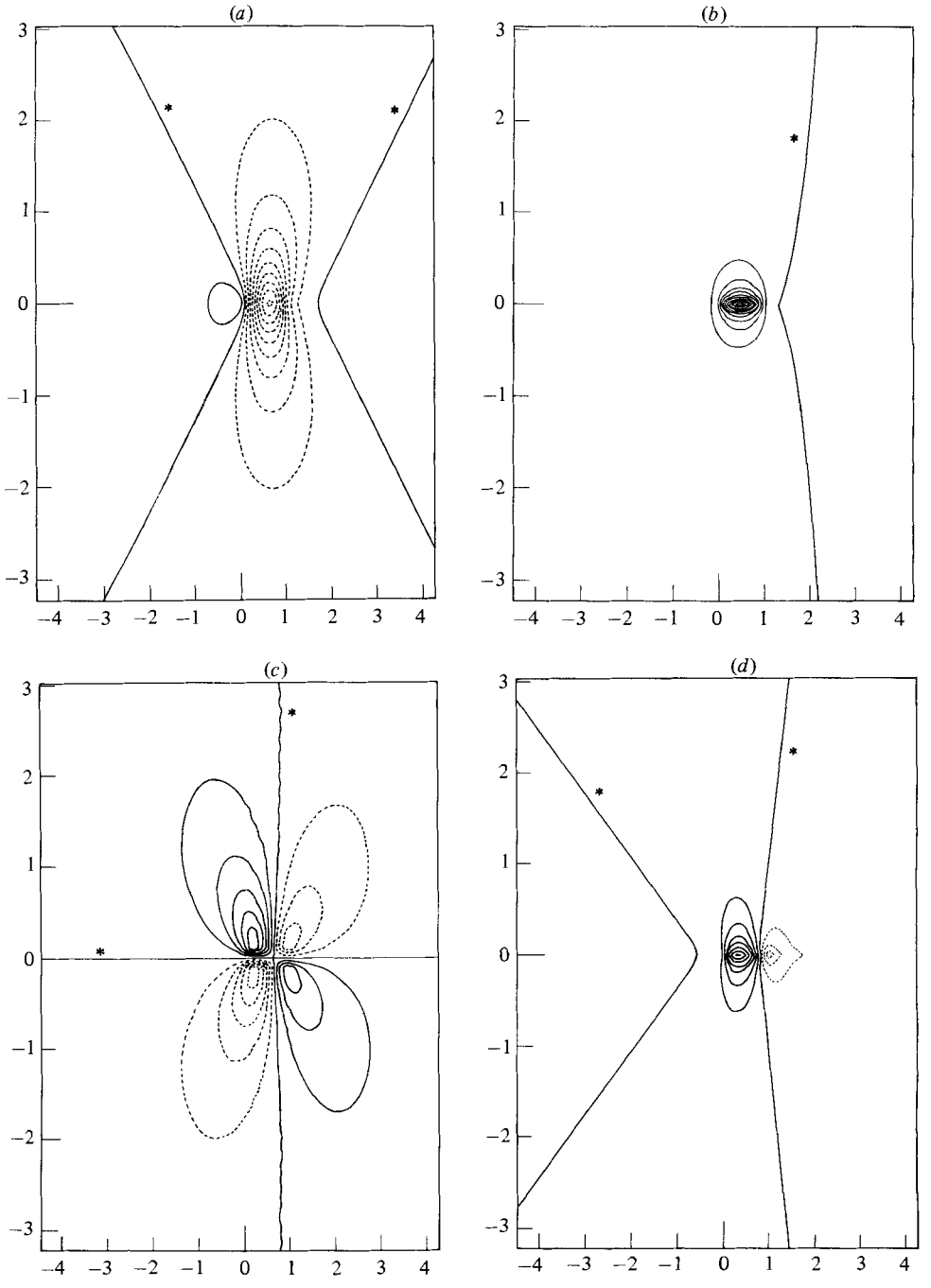

FIGURE 4. For caption see facing page.

displacement has an overshoot to a positive maximum before its fall back to zero. Thus fluid is eventually drawn towards the body surface ($\partial\delta/\partial X < 0$), in the Z-direction, whereas it moves away from the symmetry line near the body surface ($\tau_Y > 0$), although still approaching the symmetry (X, Z) plane at the edge of the viscous zone ($D < 0$). There is no evidence of the corridor phenomenon of Smith

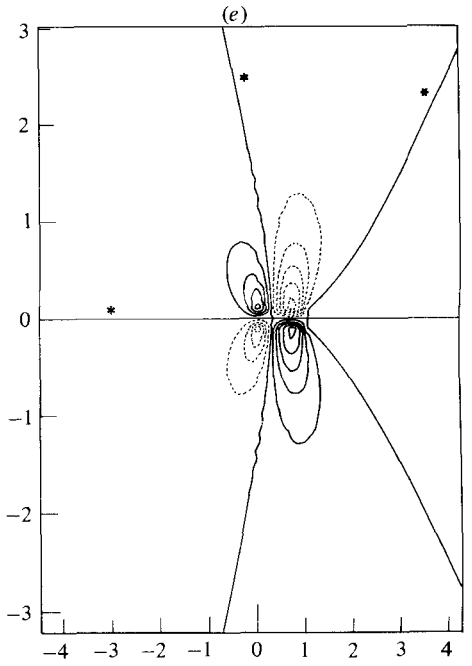

FIGURE 4. Linearized three-dimensional flow solutions for the short wing (3.4*c*). Notation, asymptotes and general secondary flow are as in figure 2. Contour values for P, $-\delta$, D, τ_X, τ_Y are: (*a*) −0.069, −0.062, −0.054, −0.046, −0.038, −0.031, −0.023, −0.015, ±0.0077, zero (*); (*b*) zero (*), 0.044, 0.087, 0.13, 0.17, 0.22, 0.26, 0.31, 0.35, 0.39, 0.44; (*c*) ±0.024, ±0.020, ±0.015, ±0.0098, ±0.0049, zero (*); (*d*) ±0.13, ±0.087, ±0.043, zero (*), 0.17, 0.22, 0.26, 0.30; (*e*) ±0.051, ±0.041, ±0.031, ±0.021, ±0.010, zero (*).

et al. (1977) far downstream. Instead, the flow returns to its original upstream state quite smoothly in general, a property that can be verified as follows from an inspection of the transforms in (3.3).

In the far field, for large X^2+Y^2, inviscid characteristics tend to dominate usually, since then in effect $k, l \to 0$. Thus (3.3*a–e*) give, for example,

$$\frac{P}{h} \propto f^*(0)\frac{X^2-Y^2}{(X^2+Y^2)^2}, \tag{3.5a}$$

$$\frac{D}{h} \propto f^*(0)\frac{-XY}{(X^2+Y^2)^2} \tag{3.5b}$$

(cf. Smith *et al.* 1977), with the wing acting as a point source ($f^*(0)$) in those cases where $\int_{-\infty}^{\infty} f(X)\,\mathrm{d}X$ is finite. The implied asymptotes for the curves of zero P, δ, τ_X, τ_Y and D are noted in the captions for figures 2–5 and agree reasonably well with the FFT calculations. The only non-uniformity in the far-field account occurs in the direct wake of the wing, when $k \to 0$ but $l \to \infty$ with $l = 0(|k|^{-\frac{1}{3}})$, in view of (3.3), i.e. as $X \to \infty$ but with $Y = O(X^{-\frac{1}{3}}) \to 0$. There viscous effects reassert their influence, but in a region that thins like $X^{-\frac{1}{3}}$ in the Y-direction while expanding (as usual) like $X^{\frac{1}{3}}$ in Z. This contrast with the flow over a three-dimensional hump is due to the two-dimensionality of the wing shape and the corresponding nature of the effective hump shape in (3.2): cf. §4.

The secondary flows induced are also of concern and are sketched in figure 2(*f*).

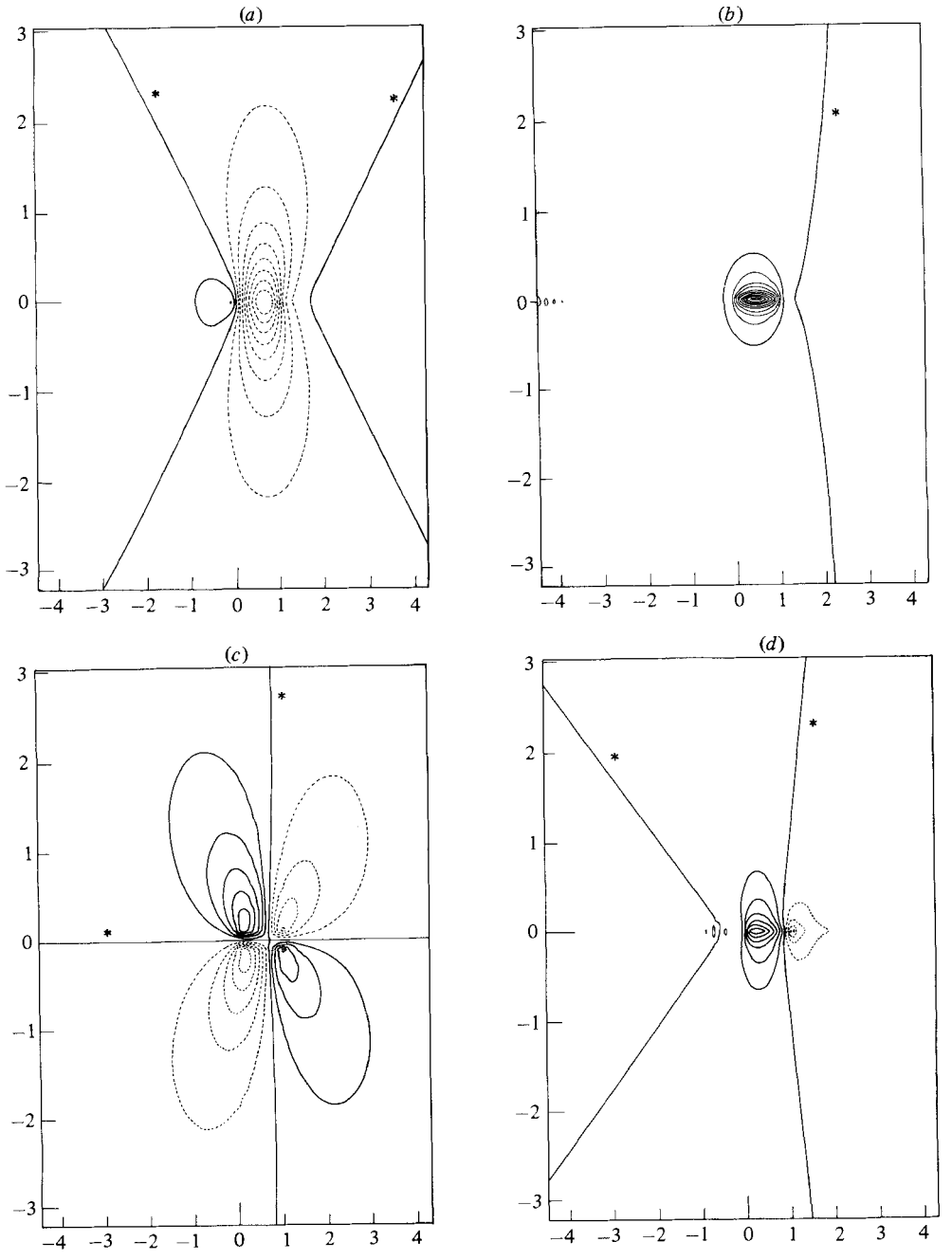

FIGURE 5. For caption see facing page.

The basis for this figure is the behaviour of δ, D, τ_X and τ_Y as X and Y vary, since these fix the flow patterns near and relatively far from the body surface. The overall trend initially is one of motion *around* the wing, as noted earlier. Thus upstream the secondary flow is away from the symmetry line but towards the body surface. Beyond the front or maximum thickness of the wing the flow then returns toward the symmetry line, but tends to be away from the body surface. Further downstream, secondary vortices are induced, producing outward motion near the body surface

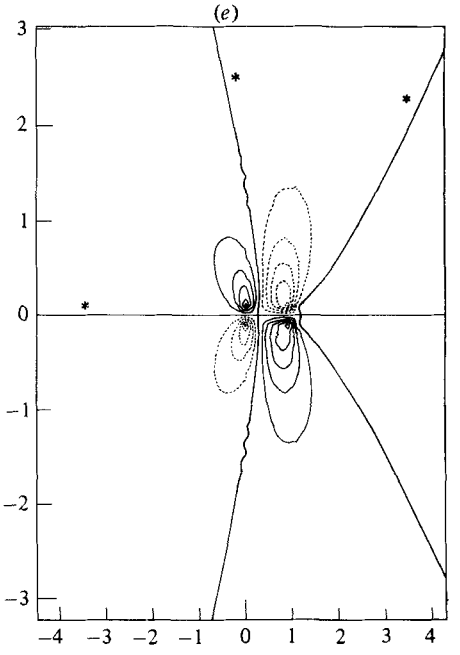

FIGURE 5. Linearized three-dimensional flow solutions for the short wing (3.4*d*). Notation, asymptotes and general secondary flow are as in figure 2. Contour values for P, $-\delta$, D, τ_X, τ_Y are: (*a*) −0.13, −0.11, −0.098, −0.082, −0.065, −0.049, ±0.033, ±0.016, zero (*); (*b*) zero (*), 0.091, 0.18, 0.27, 0.37, 0.46, 0.55, 0.64, 0.73, 0.82, 0.91; (*c*) ±0.052, ±0.042, ±0.031, ±0.021, ±0.010, zero (*); (*d*) ±0.36, ±0.27, ±0.18, ±0.09, zero (*), 0.45, 0.54; (*e*) ±0.11, ±0.089, ±0.067, ±0.045, ±0.022, zero (*).

supplied by inward motion further out and a wash of fluid *down* the wing surface/symmetry line.

Finally here we turn to the central problem of the thin flat-plate symmetric wing, taking the wing to be 'long'. Comments on shorter cases are presented in §5. The flat plate induces an interaction by means of its (Blasius) boundary layer's parabolic displacement, which acts as an effective wing thickness. The thickness is $O(Re^{-\frac{1}{2}}x^{\frac{1}{2}})$, however, and so provokes a pressure only $O(Re^{-\frac{1}{2}}x^{-\frac{1}{2}})$, or $O(Re^{-\frac{5}{16}})$, within the critical interactive length-scale at the leading edge. This is too small, by a factor $O(Re^{-\frac{1}{16}})$, to induce a nonlinear wing–body interaction, therefore. Instead a linearized response occurs, with the local wing shape being in effect exactly (3.4*b*) (for all $X > 0$) and with the gauge factor h replaced by $\beta_1 Re^{-\frac{1}{16}}$. Here $\beta_1 = 1.7208$, from the Blasius layer, and the flow structue remains intact with such a value of h. So the properties in figure 3 cover the flat-plate case also.

4. Three-dimensional wings (e.g. swept, tapered)

Sweptback or -forward wings are of considerable interest in practice, and so an investigation of the influence of sweep at a wing–body junction is desirable. Again, a smoother more three-dimensional version of the junction would seem to resemble more closely many of the geometries that are made or occur in practice. Therefore below we take the thin wing to have a general three-dimensional form

$$y = f(x, z) \tag{4.1}$$

whilst preserving the symmetry about the (x, z)-plane (figure 6).

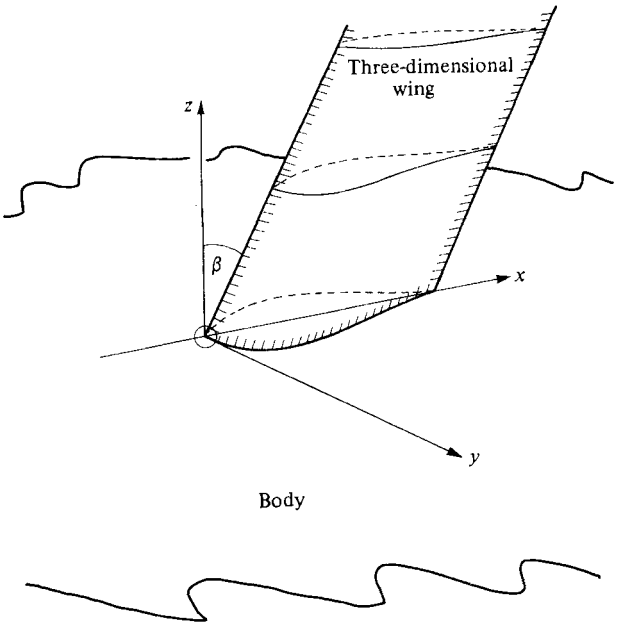

FIGURE 6. A characteristic body–three-dimensional-wing symmetric junction, with sweep (angle β) and tapering: see §4. Delta wings and other three-dimensional effects can also be dealt with.

All the critical scalings of §2 remain intact for this case, whether the wing is short or long, but the inviscid results (2.1) and (2.2a) in the upper deck need generalizing, since the three-dimensional wing condition on $\bar{p}$ is now $\partial\bar{p}/\partial Y(X,0+,\bar{z}) = -h\partial^2 f/\partial X^2(X,\bar{z})$ for tangential flow there. Here $f(x,z) \equiv h\,Re^{-\frac{3}{8}} f(X,\bar{z})$ defines the reduced wing shape in view of the critical scalings involved. So we find, after some manipulation of the solution of Laplace's three-dimensional equation (see e.g. Carrier, Krook & Pearson 1966) for $\bar{p}$, that the pressure–displacement interaction now takes the form

$$P(X,\,Y) = -\frac{1}{2\pi}\int_{-\infty}^{\infty}\int_{-\infty}^{\infty} \frac{(\partial^2 F/\partial\xi^2 - \partial^2\delta/\partial\xi^2)\,\mathrm{d}\xi\,\mathrm{d}\eta}{[(X-\xi)^2+(Y-\eta)^2]^{\frac{1}{2}}} \tag{4.2}$$

on the body surface, where the definition

$$F^{**}(k,l) = 2h\int_{X=-\infty}^{\infty}\int_{\bar{z}=0}^{\infty} \mathrm{e}^{-(k^2+l^2)^{\frac{1}{2}}\bar{z}-\mathrm{i}kX} f(X,\bar{z})\,\mathrm{d}X\,\mathrm{d}\bar{z} \tag{4.3}$$

fixes the Fourier transform of the function $F(X,\,Y)$ in terms of the known wing shape $f(X,\bar{z})$. Then (4.2) and (4.3), allied with the three-dimensional boundary-layer equations in (2.2b–g), which still hold in the lower deck on the body surface, determine the local nonlinear flow interaction. Here in fact (4.3) defines the effective hump shape F, just as in §3.

For linearized motion where the parameter h is small we may use (4.3) to determine F, for a given three-dimensional wing shape f, and then as in §3 appeal directly to the results for flow past humps in Smith *et al.* (1977). Hence it follows that the solutions (3.3a–e) are retrieved, but with F^{**} now given by (4.3). Two main examples of interest are the swept wing and the tapered wing or junction. For the swept wing first, if the sweep angle is β, where $f(X,\bar{z}) = g(X-\bar{z}\tan\beta)$ for $X > \bar{z}\tan\beta$, $f(X,\bar{z}) = 0$

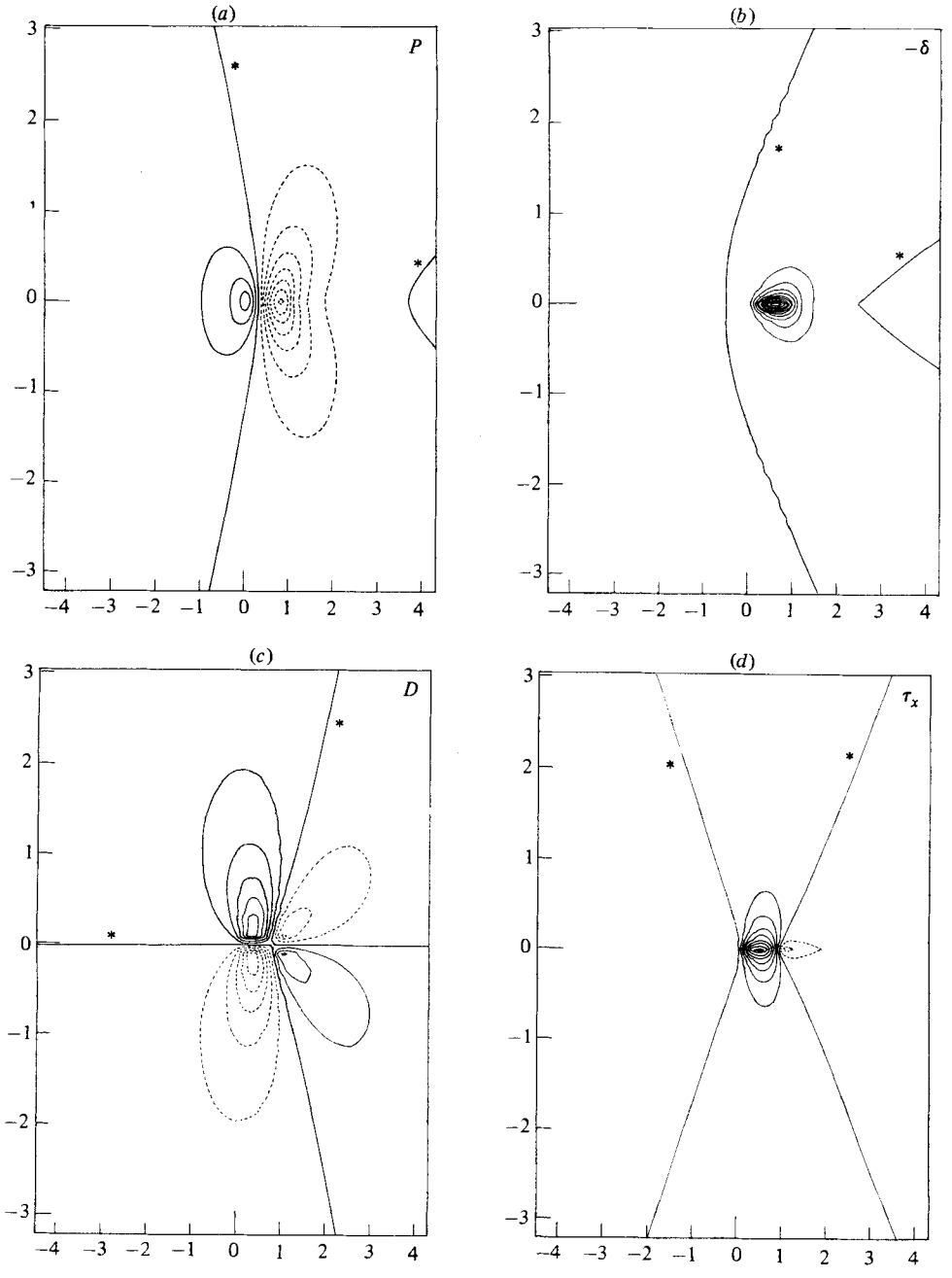

FIGURE 7. For caption see page 209.

for $X < \bar{z}\tan\beta$, and $g(X)$ is the base of the wing shape adjoining the body surface at $\bar{z} = 0+$, (4.3) yields

$$\frac{F^{**}(k,l)}{h} = \frac{2g^*(k)}{ik\tan\beta + (k^2+l^2)^{\frac{1}{2}}}. \tag{4.4}$$

Combined with (3.3*a–e*), (4.4) then yields the solutions for the corresponding interaction properties presented in figure 7, for a particular base shape $g(X)$. Here

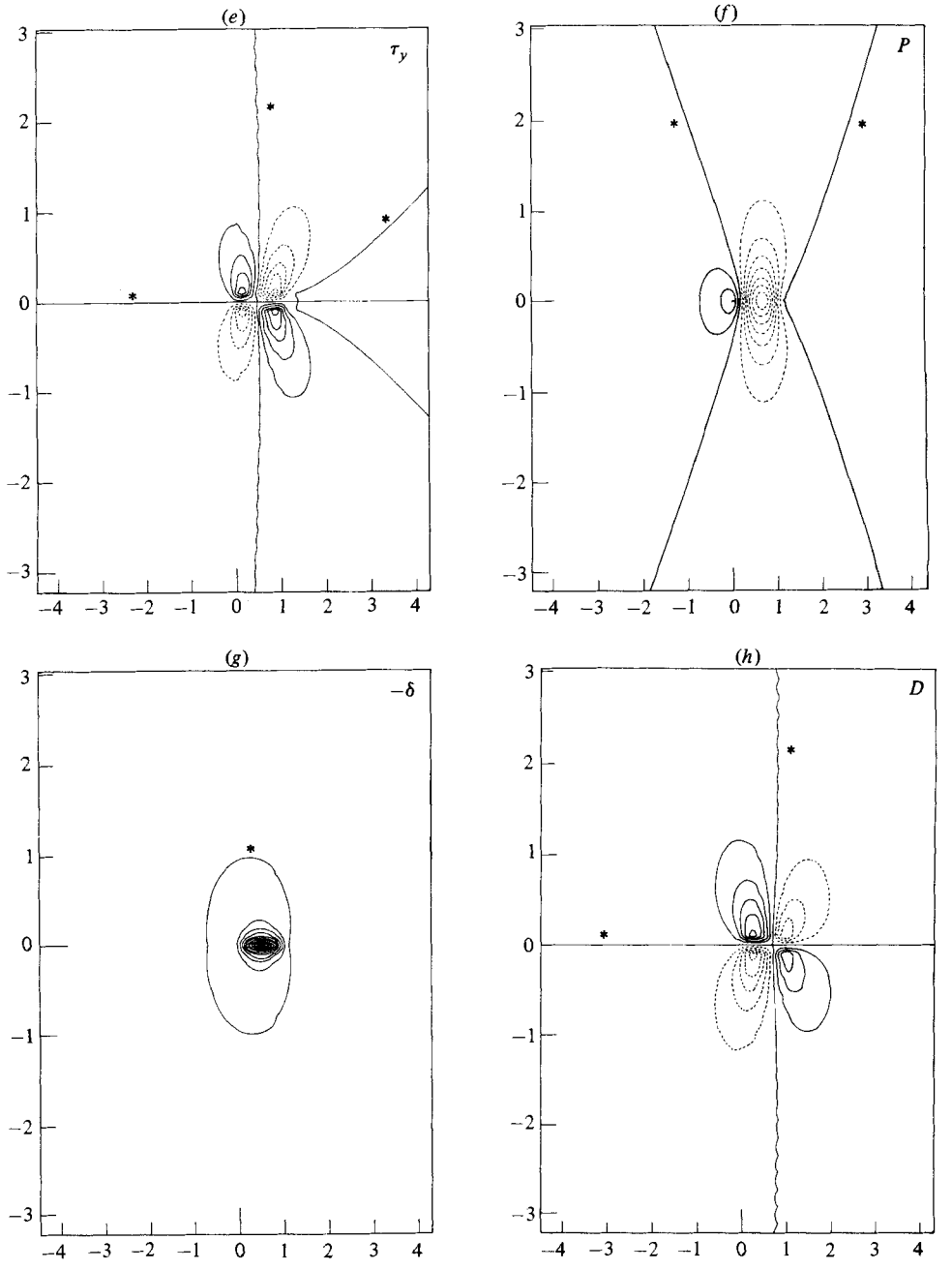

FIGURE 7. For caption see facing page.

again no corridor effect emerges in the flow far downstream on the present scale. Secondly, for the tapered wing typically we have $f(X,\bar{z}) = g_1(X)\,g_2(\bar{z})$ with $g_2(\bar{z})$ controlling the degree of tapering in the $\bar{z}$-direction away from the junction. As an example we take the exponential form $g_2(\bar{z}) = \exp(-\sigma\bar{z})$ $(\bar{z} > 0)$, with σ a positive constant, for which (4.3) then gives

$$\frac{F^{**}(k,l)}{h} = \frac{2g_1^*(k)}{\sigma + (k^2+l^2)^{\frac{1}{2}}}. \tag{4.5}$$

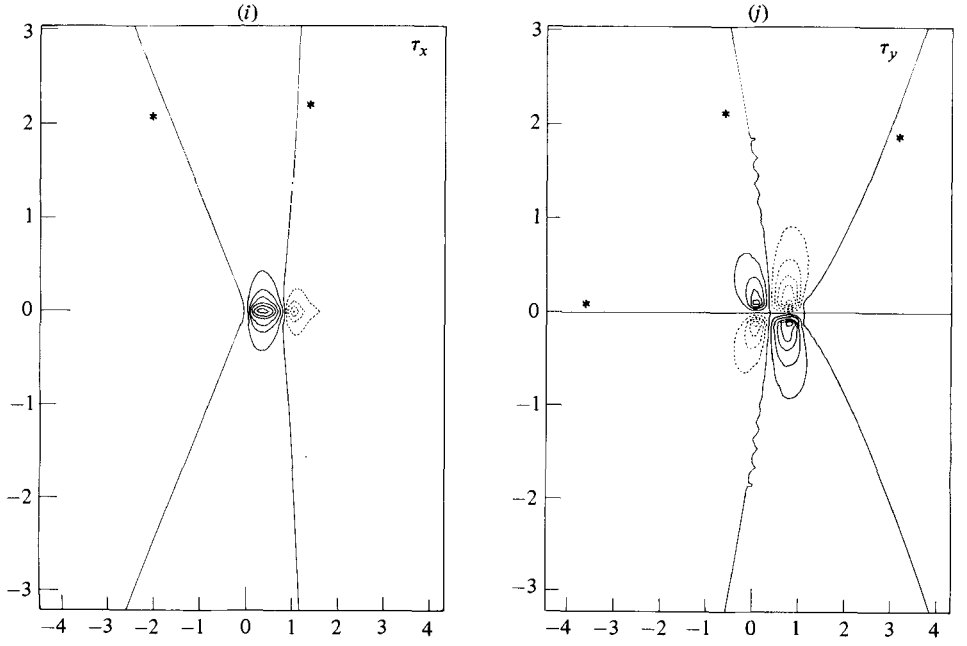

FIGURE 7. Linearized flow solutions for the examples of three-dimensional wings considered in §4, the swept wing ((*a*)–(*e*)) and the tapered wing ((*f*)–(*j*)). The contour values are: (*a*) −0.050, −0.043, −0.036, −0.028, ±0.021, ±0.014, ±0.0071, zero (*); (*b*) zero (*), 0.039, 0.077, 0.12, 0.15, 0.19, 0.23, 0.27, 0.31, 0.35, 0.39; (*c*) ±0.023, ±0.018, ±0.014, ±0.0091, ±0.0046, zero (*); (*d*) ±0.062, ±0.031, zero (*), 0.094, 0.12, 0.16, 0.19, 0.22, 0.25; (*e*) ±0.046, ±0.037, ±0.028, ±0.018, ±0.0092, zero (*); (*f*) −0.037, −0.032, −0.026, −0.021, ±0.016, ±0.011, ±0.0053, zero (*); (*g*) zero (*), 0.033, 0.065, 0.098, 0.13, 0.16, 0.20, 0.23, 0.26, 0.29, 0.33; (*h*) ±0.019, ±0.016, ±0.012, ±0.0078, ±0.0039, zero (*); (*i*) ±0.13, ±0.10, ±0.066, ±0.033, zero (*), 0.17, 0.20; (*j*) ±0.042, ±0.034, ±0.025, ±0.017, ±0.0084, zero (*). The sweep angle is 45°, with $g(X) = X(1-X)$ for $0 < X < 1$, $g(X) = 0$ otherwise, in (*a*)–(*e*). The taper in (*f*)–(*j*) is for $\sigma = 2$, with $g_1(X) = X(1-X)$ for $0 < X < 1$, $g_1(X) = 0$ otherwise.

Figure 7 also shows the interactive solutions in this case, for a particular wing base shape $g_1(X)$. Because of the action of the σ-term in (4.5), a corridor effect for $Y = O(1)$ is found, analytically and numerically, to be present downstream now as X increases, but its properties are different from those of Smith *et al.*, since here it involves no change in the orders of magnitude of P, δ, D, τ_X and τ_Y. There is only a slight logarithmic singularity as $Y \to 0$, which is smoothed out in the thinner zone $O(X^{-\frac{1}{3}})$ width mentioned earlier. This demonstrates to some extent the controlling effect of the wing's local three-dimensionality, close to the junction, on the interactive three-dimensional motion induced at the body surface. The secondary flows induced can also be surmised from figure 7.

Two unusual aspects of these flow solutions compared with those of §3 are, first, the occurrence of a positive displacement effect in most of the flow ahead of each of the three-dimensional wings, before an abrupt decrease takes place immediately before the wing; and, secondly, the closed loops of constant displacement found for the junction with a tapered wing. It is interesting also that sweep angles β of order unity can be accommodated in the theory. The far fields can be deduced as for the two-dimensional wings considered earlier.

5. Further comments, comparisons and larger-scale features

The model studied above for the wing–body junction takes a rather simplistic geometry comprising a thin two- or three-dimensional wing (figures 1 and 6) protruding normally from a flat body surface, with or without sweep. Yet such a model would seem to provide a reasonable *first* step towards understanding analytically the three-dimensional flow interactions possible. Indeed the flat-plate example noted in §3 may be regarded as an obvious central problem to study. One would perhaps not expect these thin-wing models to bear much relation to the bluff-wing–body configurations examined experimentally (e.g. East & Hoxey 1968; Peake *et al.* 1965; Shabaka & Bradshaw 1981), but nevertheless the measure of agreement on certain flow features is surprisingly good. In particular the linearized solutions always show two maximum local deficits taking place in the streamwise (X) surface shear stress on the body, just ahead of and beyond the front of the wing, on the axis of symmetry, which suggests that regular separation or flow reversal would tend to occur there first, in the nonlinear regime. That, allied with the corresponding Y surface-shear-stress patterns, forms a fairly clear connection with the experimental observations (see references above) of a separation line starting upstream of the wing, and bending round it, and of separation downstream. Also the strong secondary-flow patterns found here appear to be sensible physically and to tie in generally with those reported in the above references, as fluid is forced to move around the wing. Specifically, for turbulent-flow experiments, figure 3 of Shabaka & Bradshaw (1981) compares most favourably with our theoretical finding (figures 2–5) of a pronounced downwash on the wing sufficiently far beyond the leading edge. For laminar flow the experiments of Peake *et al.* (1965), e.g. their figures 11–13 and 17, also give crossflows similar to those found theoretically here. Qualitative agreement continues to hold in comparisons with the classical boundary layer calculations of Zhu (1982) concerning both the separation line upstream (see his figures 1, 5 and 23) and the cross-flow (his Figures 8, 10, 28 and 29), although there is a puzzling feature in the displacement thickness (his figure 11), which shows an increase ahead of the wing rather than the decreases predicted theoretically (see our figures above). The further experiments reported by Zhu also tend to agree qualitatively with the present theoretical study.

In view of the particularly promising measure of possible agreement overall above it would be very interesting to see the results of a numerical study of the nonlinear regime (2.2a–g) holding when h is $O(1)$ or larger. Possible numerical schemes for this three-dimensional problem are described by Burggraf & Duck (1983) and Smith (1983). Some other improvements in the models taken can be made also, for instance (a) by adding in a hump shape on the body surface to produce a smoother junction, (b) by considering wings at nonzero angles of incidence, (c) by assuming three-dimensional oncoming flow both along the body surface and away from it, and (d) by considering wings with nonzero angles of dip. Here, in (b), the critical angle of incidence α_1 (the angle between the plane of the wing and the (x, z)-plane) is small, of order $Re^{-\frac{7}{16}}$, for a long thin wing since the induced pressure is of order $\alpha_1 x^{-\frac{1}{2}}$ near the leading edge; whereas the effect of an angle of dip α_2 (the angle between the body surface and the plane of the wing), in (d) above, is less drastic in the sense that the flow structures found earlier in §§2–4 remain appropriate even for $O(1)$ values of α_2, if the wing is thin. Both incidence and dip introduce nonsymmetry into the wing–body interaction, however.

The development of the motion downstream beyond the triple-deck at the leading edge is also of concern. Many studies have been made (e.g. Zamir 1968; Rubin &

Grossman 1971, Desai & Mangler 1974) of the well-developed similarity flow believed to be achieved only as $x \to \infty$ in a configuration such as that in figure 1, e.g. the flat-plate wing. But little or no research into the developing flow properties holding for finite $x > 0$ is evident yet. There the main flow structure becomes at first sight a relatively simple one, with Blasius boundary layers of typical thickness $O(Re^{-\frac{1}{2}})$ (but different origins) astride the wing and the body except in a classical $O(Re^{-\frac{1}{2}})$ by $O(Re^{-\frac{1}{2}})$ zone (Z1, say) near the x-axis where y- and z-diffusion become comparable. This picture emerges from the leading-edge properties of §§2–4 as $X \to +\infty$, since there viscous interactive effects concentrate in a zone (Z2) whose Z-scale increases like $X^{+\frac{1}{3}}$ but whose Y-scale decreases like $X^{-\frac{1}{3}}$ (see the far field in §3). So the y- and z-scales of Z2 are then respectively of orders $Re^{-\frac{3}{8}}(Re^{\frac{3}{8}}x)^{-\frac{1}{3}}$ and $Re^{-\frac{5}{8}}(Re^{\frac{3}{8}}x)^{\frac{1}{3}}$, and both become $O(Re^{-\frac{1}{2}})$ as x rises to become $O(1)$. Thus zone Z2 merges into zone Z1 downstream. It is striking that the thickness of Z1 in the y-direction must therefore appear unbounded ($\propto x^{-\frac{1}{3}}$) initially, as $x \to 0+$. The remainder of the triple-deck interaction, outside zone Z2, has less influence downstream, but its effects do persist nonetheless, and they force a secondary flow in the two Blasius layers in $x > 0$. This interactive secondary flow is not mentioned in previous studies.

In addition, in cases where the leading-edge interaction produces a corridor (wherein $Y = O(1)$) downstream, an extra $O(Re^{-\frac{3}{8}})$ by $O(Re^{-\frac{3}{8}})$ zone is produced along the x-axis for $x > 0$, forming a buffer between the classical zone Z1 and the Blasius layers. This corridor, which has been observed experimentally in flow over humps, could have a significant impact on the flow downstream.

Finally, again for the flat-plate wing, it is of practical interest to examine the trailing-edge motion. Suppose the wing has chord length L, of order unity (see figure 8). For $0 < x < L$, and outside Z1, the two Blasius layers BL1 and BL2 grow along the wing and the body surface, after the mainly linear adjustment (§3) near the leading edge $x = 0$. Near the trailing edge at $x = L$ more triple-deck interaction therefore comes into operation. It has a predominantly two-dimensional form (as determined by Jobe & Burggraf 1974) on most of the wing, the prime exception being at distances z of order $Re^{-\frac{3}{8}}$ from the body surface, where the flow interaction must become three-dimensional again and nonlinear for *both* the wing and body motions. There, first, the flow adjoining the body surface satisfies the three-dimensional boundary-layer equations (2.2*b–g*) again, but with

$$\lambda, X \quad \text{replaced by} \quad \lambda_2, \tilde{X} \equiv Re^{\frac{3}{8}}(x-L), \tag{5.1}$$

respectively, where λ_2 is the incident reduced skin friction of BL2 as $x \to L-$, and $0 < \lambda_2 < \lambda$. Secondly, the viscous layer on the wing ($\tilde{X} < 0$) and in its wake ($\tilde{X} > 0$) is also controlled by (2.2*b–d,f,g*), subject to the replacements

$$(U, V, W, P, \delta, X, Y, Z, \lambda) \to (\hat{U}, \hat{W}, \hat{V}, \hat{P}, \hat{\delta}, \tilde{X}, \tilde{z}, \hat{Y}, \lambda_1) \tag{5.2}$$

for the rotation of axes, and subject to the usual lower-deck scalings again. Here $\lambda_1 > 0$ is the reduced skin friction of BL1 at $x = L-$, and instead of (2.2*e*) we have the trailing-edge conditions

$$\hat{U} = \hat{W} = \hat{V} = 0 \quad \text{at} \quad \hat{Y} = 0, \quad \tilde{X} < 0, \tag{5.3a}$$

$$\frac{\partial \hat{U}}{\partial \hat{Y}} = \frac{\partial \hat{W}}{\partial \hat{Y}} = \hat{V} = 0 \quad \text{at} \quad \hat{Y} = 0, \quad \tilde{X} > 0. \tag{5.3b}$$

The interaction between the two nonlinear layers of (5.1) and (5.2) arises through their respective unknown pressures and displacements, $P(\tilde{X}, Y)$ and $\delta(\tilde{X}, Y)$ on the body

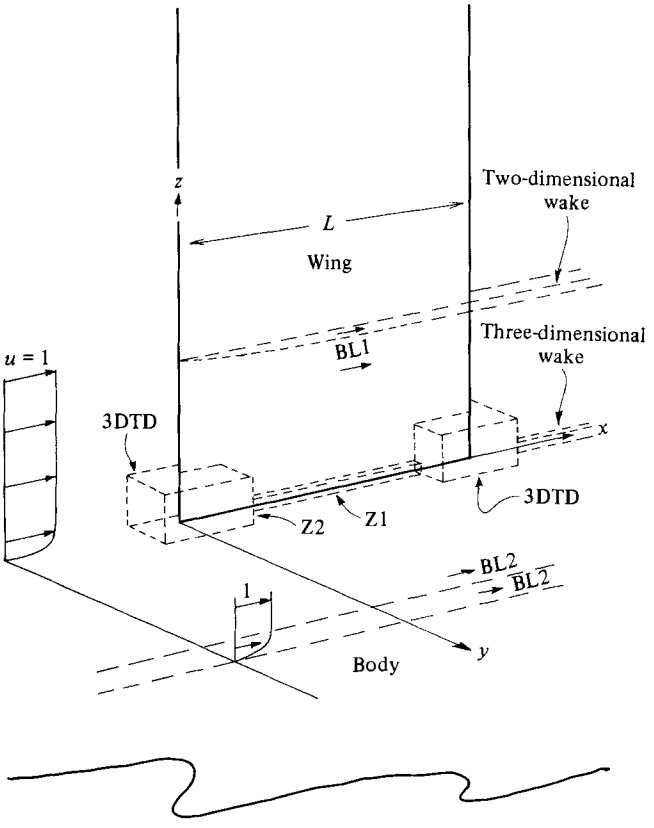

FIGURE 8. Flow past the junction of a symmetric two-dimensional flat-plate wing, chord L = $O(1)$, and a flat body surface, showing the flow structure (dashed lines). This is dominated by the leading-edge and trailing-edge three-dimensional triple decks (3D TD), the thinner classical two-dimensional boundary layers BL1, BL2 and classical three-dimensional corner boundary layer Z1, and the thin two- and three-dimensional wakes. See §5. Similar flow structures can apply for thicker and/or three-dimensional wing–body junctions.

and $\hat{P}(\tilde{X}, \bar{z})$ and $\hat{\delta}(\tilde{X}, \bar{z})$ on the wing, in scaled terms. These are linked via the three-dimensional potential flow in the upper deck, which requires that

$$P(\tilde{X}, Y) = -\frac{1}{2\pi}\int_{-\infty}^{\infty}\int_{-\infty}^{\infty} \frac{(\partial^2 F/\partial\xi^2 - \partial^2\delta/\partial\xi^2)\,\mathrm{d}\xi\,\mathrm{d}\eta}{[(\tilde{X}-\xi)^2+(Y-\eta)^2]^{\frac{1}{2}}}, \tag{5.4a}$$

$$\hat{P}(\tilde{X}, \bar{z}) = -\frac{1}{2\pi}\int_{-\infty}^{\infty}\int_{-\infty}^{\infty} \frac{(\partial^2 \hat{F}/\partial\xi^2 - \partial^2\hat{\delta}/\partial\xi^2)\,\mathrm{d}\xi\,\mathrm{d}\nu}{[(\tilde{X}-\xi)^2+(\bar{z}-\nu)^2]^{\frac{1}{2}}}, \tag{5.4b}$$

where $F(\tilde{X}, Y)$ and $\hat{F}(\tilde{X}, \bar{z})$ are given by the transforms

$$F^{**}(k, l) = 2\int_{\tilde{X}=-\infty}^{\infty}\int_{\bar{z}=0}^{\infty} \mathrm{e}^{-(k^2+l^2)^{\frac{1}{2}}\bar{z}-\mathrm{i}k\tilde{X}}\,\delta(\tilde{X}, \bar{z})\,\mathrm{d}\tilde{X}\,\mathrm{d}\bar{z}, \tag{5.4c}$$

$$\hat{F}^{**}(k, m) = 2\int_{\tilde{X}=-\infty}^{\infty}\int_{Y=0}^{\infty} \mathrm{e}^{-(k^2+m^2)^{\frac{1}{2}}Y-\mathrm{i}k\tilde{X}}\,\delta(\tilde{X}, Y)\,\mathrm{d}\tilde{X}\,\mathrm{d}Y, \tag{5.4d}$$

similar to §4. In consequence the wing and body surface flows near the trailing edge affect each other about equally, in general (cf. the leading edge, in §§2–4, where the major interaction is one-way only); and a challenging, nonlinear, *coupled* three-

dimensional problem is posed for the local flow adjustment. Some useful and analytical properties can be derived however if the wing is relatively short, so that L is small. For then the Blasius layer BL1 has its skin friction enhanced, since

$$\lambda_1 = \tau_1 L^{-\frac{1}{2}}, \tag{5.5}$$

where $\tau_1 = 0.33206...$. Hence the three-dimensional triple deck associated with the wing surface, in (5.2), shrinks, by factors $L^{\frac{5}{8}}$ in all the $\tilde{X}$-, Y- and $\bar{z}$-directions, and for $\bar{z}$ of order unity the trailing-edge motion becomes virtually planar (and as in Jobe & Burggraf 1974). Indeed, for $\tilde{X}$, Y and $\bar{z}$ all $O(1)$, i.e. in the three-dimensional upper deck which controls the body surface motion, we have potential flow past the classical planar displacement

$$\hat{\delta}(\tilde{X}, \bar{z}) = \begin{cases} 0 & (\tilde{X} < 0), \quad (5.6a) \\ -\beta_1 L^{\frac{1}{8}} \tilde{X}^{\frac{1}{2}} & (\tilde{X} > 0), \quad (5.6b) \end{cases}$$

where L is small. Here β_1 is a finite positive constant, and (5.6b) describes the Goldstein (1930) near wake. The irregularity at $\tilde{X} = 0\pm$ in (5.6a, b) is smoothed out when $\tilde{X}$ is smaller, of order $L^{\frac{5}{8}}$. For $\tilde{X} = O(1)$ the wing–body interaction of (5.1)–(5.4d) becomes mostly one-way again, and linear, since (5.4a) now yields (2.2a) with

$$hf(X) \to \hat{\delta}(\tilde{X}, \bar{z}). \tag{5.6c}$$

The reverse effect, of the body on the wing flow, is now diminished. Hence the three-dimensional traling-edge adjustment considered reduces to the linearized analysis of §3, with $h = \beta_1 L^{\frac{1}{8}}$ small. The corresponding solutions for the body surface flow near the trailing edge are presented in figure 9. As expected, they are similar to those of §3 except that the $-$ sign in (5.6b) alters all the signs involved. Thus, on the body surface, we obtain

increased displacement,
decreased pressure,
increased streamwise shear,
inward crossflow shear
} ahead of the trailing edge, close to the junction; (5.7a)

decreased displacement,
increased pressure,
decreased streamwise shear,
outward crossflow shear
} in the wake, almost directly behind the wing. (5.7b)

This tends to confirm the roughly equal but opposite effects of the leading and trailing edges described in §3. Also, there is no corridor, and the $\tilde{X}^{-\frac{1}{3}}$ narrowing downstream is covered by earlier comments. Note that the above applies for L small but greater than $O(Re^{-\frac{3}{8}})$, so that the trailing-edge interaction remains distinct from the earlier one at the leading edge. It also applies near the trailing edges of short flat-plate wings like those in §3 if the scaled chord length L there is large.

The displacement decrease in (5.7b), which is pronounced, and the associated pressure increase there, would appear to agree with physical expectations for the flow behind the wing.

A computational treatment applied to the nonlinear version of the trailing-edge

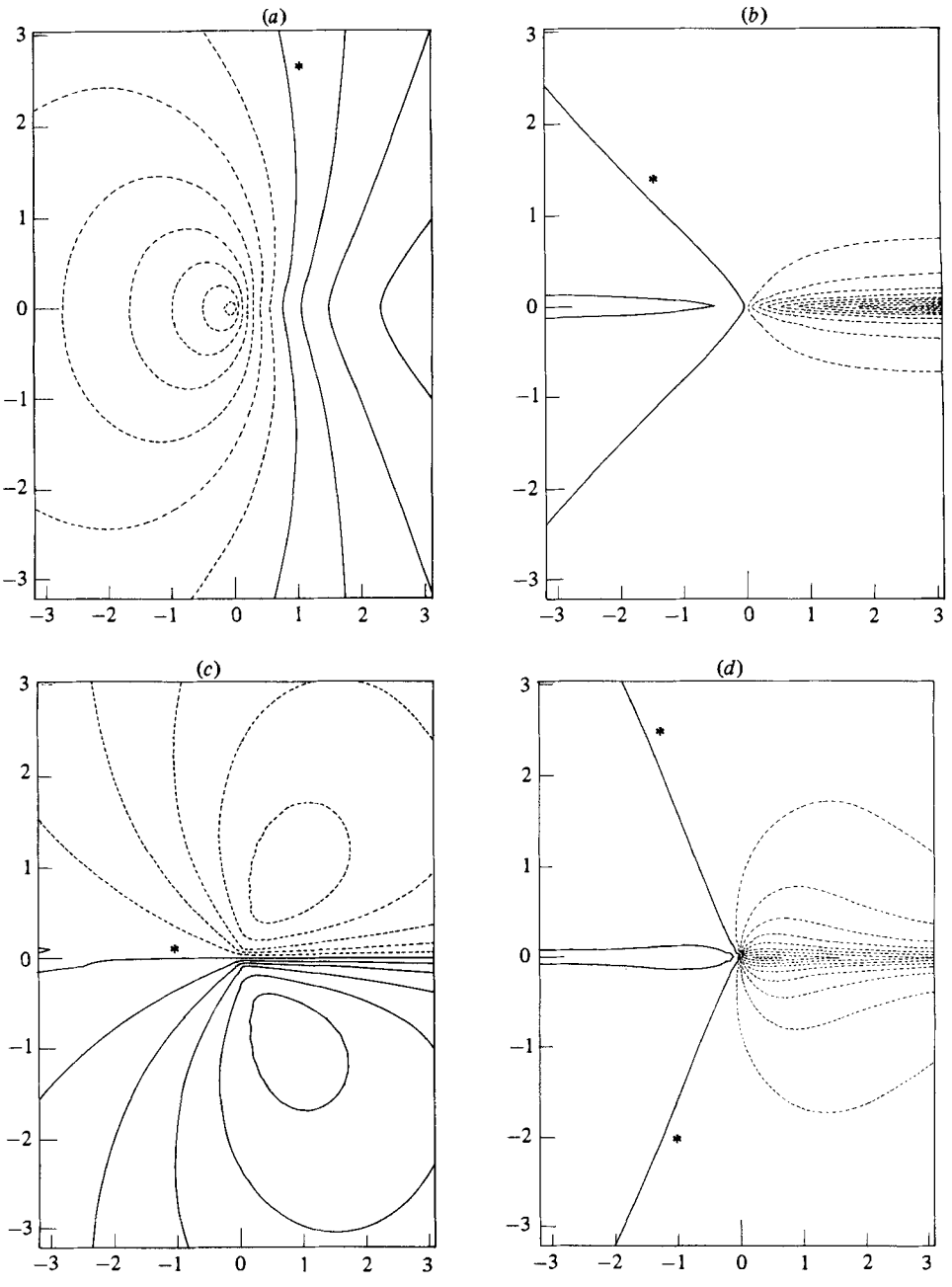

FIGURE 9. For caption see facing page.

junction flow in (5.1)–(5.4*d*) would be of considerable interest, possible computational methods again being those of Burggraf & Duck (1983) and Smith (1983). Experimental studies of the central, flat-plate, wing–body-junction model (figure 8) could also be an aid to furthering our theoretical and physical understanding.

J.G. wishes to thank the S.E.R.C. for financial support. We both thank Mr J. H. B. Smith and Prof. P. Bradshaw for kindly pointing out some helpful references to us.

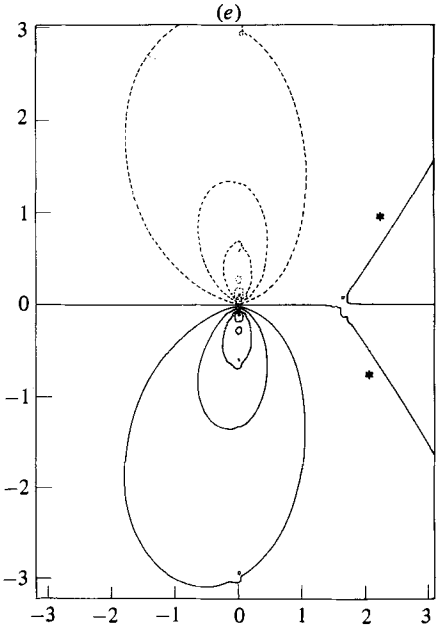

FIGURE 9. Linearized three-dimensional solutions for P, $-\delta$, D, τ_X, τ_Y in (*a*)–(*e*) respectively near the trailing edge of the wing–body junction when the chord L is small (see §5). The axes are $\bar{X}$, Y. Contour values are : (*a*) −0.22, −0.19, −0.16, −0.13, ±0.096, ±0.064, ±0.032, zero (*); (*b*) −2.6, −2.3, −2.0, −1.7, −1.4, −1.1, −0.85, −0.57, ±0.28, zero (*); (*c*) ±0.16, ±0.13, ±0.096, ±0.064, ±0.032, zero (*); (*d*) −0.75, −0.67, −0.58, −0.50, −0.42, −0.33, −0.25, −0.17, ±0.083, zero (*); (*e*) ±0.19, ±0.15, ±0.12, ±0.077, ±0.039, zero (*).

REFERENCES

BURGGRAF, O. R. & DUCK, P. W. 1983 In *Proc. 2nd Symp. Numer. and Phys. Aspects of Aerodyn. Flows, Long Beach, Calif.*

CARRIER, G. F., KROOK, M. & PEARSON, C. E. 1966 *Functions of a Complex Variable.* McGraw-Hill.

DESAI, S. S. & MANGLER, K. W. 1974 *RAE Tech. Rep.* 74062.

EAST, L. F. & HOXEY, R. P. 1968 *RAE Tech. Rep.* 68161.

GOLDSTEIN, S. 1930 *Proc. Camb. Phil. Soc.* **26**, 1.

JOBE, C. E. & BURGGRAF, O. R. 1974 *Proc. R. Soc. Lond.* A **340**, 91.

KITCHENS, C. W., GERBER, N., SEDNEY, R. & BARTOS, J. M. 1983 *AIAA J.* **21**, 856.

MCDONALD, H. & BRILEY, W. R. 1982 In *Proc. 1st. Symp. Numer. and Phys. Aspects of Aerodyn. Flows, Long Beach, Calif.* Springer.

MEHTA, R. D., SHABAKA, I. M. M. A. & BRADSHAW, P. 1982 In *Proc. 1st. Symp. Numer. and Phys. Aspects of Aerodyn. Flows, Long Beach, Calif.* Springer.

MEHTA, R. D., SHABAKA, I. M. M. A., SHIBL, A. & BRADSHAW, P. 1983 *AIAA Paper* 83–0378, *presented at AIAA 21st Aerosp. Sci. Meeting, Jan. 1983, Reno, Nevada.*

PEAKE, D. J., GALWAY, R. D. & RAINBIRD, W. J. 1965 *Natl Res. Counc. Can. Aero. Rep.* LR-446(NRC 8925).

RUBIN, S. G. & GROSSMAN, B. 1971 *Q. Appl. Maths* **29**, 169.

SHABAKA, I. M. M. A. & BRADSHAW, P. 1981 *AIAA J.* **19**, 131.

SMITH, F. T. 1983 *Utd Tech. Res. Center, E. Hartford, Conn., Rep.* UTRC-83-46.

SMITH, F. T., SYKES, R. I. & BRIGHTON, P. W. M. 1977 *J. Fluid Mech.* **83**, 163.

VAN DYKE, M. 1964 *Perturbation Methods in Fluid Mechanics.* Academic.

ZAMIR, M. 1968 Ph.D. thesis, University of London.

ZHU, Z. 1982 *DFVLR Rep.* FB 82–29.